



Article

Building Orientation and Post Processing of Ti6Al4V Produced by Laser Powder Bed Fusion Process

Rosaria Rovetta ¹, Paola Ginestra ^{1,*}, Rosalba Monica Ferraro ², Keren Zohar-Hauber ³, Silvia Giliani ²
and Elisabetta Ceretti ¹

¹ Department of Mechanical and Industrial Engineering, University of Brescia, Via Branze 38, 25123 Brescia, Italy

² Institute of Molecular Medicine “Angelo Nocivelli”, Department of Molecular and Translational Medicine, University of Brescia, 25123 Brescia, Italy

³ Metallurgical and Powders Technologies Lab, Institute of Metals, Technion City, Haifa 320003, Israel

* Correspondence: paola.ginestra@unibs.it

Abstract: Laser powder bed fusion, particularly the selective laser melting (SLM), is an additive manufacturing (AM) technology used to produce near-net-shaped engineering components for biomedical applications, especially in orthopaedics. Ti6Al4V is commonly used for producing orthopaedic implants using SLM because it has excellent mechanical qualities, a high level of biocompatibility, and corrosion resistance. However, the main problems associated with this process are the result of its surface properties: it has to be able to promote cell attachment but, at the same time, avoid bacteria colonization. Surface modification is used as a post-processing technique to provide items the unique qualities that can improve their functionality and performance in particular working conditions. The goal of this work was to produce and analyse Ti6Al4V samples fabricated by SLM with different building directions in relation to the building plate (0° and 45°) and post-processed by anodization and passivation. The results demonstrate how the production and post processes had an impact on osteoblast attachment, mineralization, and osseointegration over an extended period of time. Though the anodization treatment result was cytotoxic, the biocompatibility of as-built specimens and specimens after passivation treatment was confirmed. In addition, it was discovered that effective post-processing increases the mineralization of these types of 3D-printed surfaces.

Keywords: laser powder bed fusion; building orientation; anodization; etching; titanium; osseointegration



Citation: Rovetta, R.; Ginestra, P.; Ferraro, R.M.; Zohar-Hauber, K.; Giliani, S.; Ceretti, E. Building Orientation and Post Processing of Ti6Al4V Produced by Laser Powder Bed Fusion Process. *J. Manuf. Mater. Process.* **2023**, *7*, 43. <https://doi.org/10.3390/jmmp7010043>

Academic Editor: Steven Y. Liang

Received: 3 January 2023

Revised: 27 January 2023

Accepted: 6 February 2023

Published: 7 February 2023



Copyright: © 2023 by the authors. Licensee MDPI, Basel, Switzerland. This article is an open access article distributed under the terms and conditions of the Creative Commons Attribution (CC BY) license (<https://creativecommons.org/licenses/by/4.0/>).

1. Introduction

The demand for orthopaedic implants is estimated to increase rapidly over the coming decade. In order to support damaged tissues and bones and improve patient comfort, researchers in the field of orthopaedic implant production have developed a variety of solutions [1,2]. Numerous advantages come with these orthopaedic implant solutions, including relatively low cost, less discomfort, and quick recovery. In future years, worldwide orthopaedic implant demand will move towards less invasive and more affordable techniques for joint replacement surgery. In order to satisfy this demand, use of new production technologies is crucial [3–6].

Additive manufacturing (AM) is a modern and continuously evolving technology. Better known as 3D printing, AM empowers researchers to make parts directly from digital designs. AM has made it easier to make new three-dimensional parts in low to medium volumes. Because of the ability of AM to produce highly customized products, the use of different AM technologies has grown significantly in the biomedical field, especially orthopaedics [7,8]. An integral part of using this technology is choosing the most suitable materials as well as the most suitable AM techniques [9,10]. The mechanical qualities of titanium and its alloys, particularly those provided by the surface, such as corrosion resistance

and bioactivity, make them ideal materials for orthopaedic implants [11]. The Ti6Al4V alloy, in particular, is frequently utilised for bone replacement due to its ability to improve the adhesion between native tissue and the implanted material [12–17].

Printing titanium alloys has been successfully accomplished using selective laser melting (SLM), one of the most widely used AM techniques [18]. In the SLM process, metallic powders are uniformly spread across the build plate using a roller or wiper and fused together selectively according to the CAD model by a high energy laser beam in a protective atmosphere [19,20]. SLM offers a great chance to create sophisticated bespoke implants with the desired inner structure and surface morphology [21–23]. The final properties of the product depend not only on the source file, typically a CAD scanned by the patient, but also on the process parameters. A previous study has summarized the way in which, in the manufacturing of Ti6Al4V with SLM process, factors such as laser power, scanning speed, and powder bed temperature have a substantial impact on product quality and produce varying degrees of confidence [24]. More precisely, in terms of the macro-scale, the process parameters have limited impact on geometry, in contrast with their importance at the micro scale, particularly for surface quality, which is crucial for biomedical applications [25–27].

There is typically insufficient osseointegration between the implant and host bone tissue as a result of the product surface. In fact, one of the most important issues with an *in vivo* implant is a weak cellular adhesion against bacterial proliferation [28–30]. According to this interesting perspective, implants with a certain surface topography have a high potential for improving osseointegration [31]. Surface micro/nanostructures can therefore be created by surface modification to improve the interaction between the implant and the cell colonization, such as migration, proliferation, and differentiation [32,33]. Many surface modification approaches may be used to increase Ti6Al4V bioactivity and bone–implant compatibility [34–36]. First and foremost among these is process parameter optimization, which allows the tunability of the building angle followed by chemical and physical modification with anodization and passivation, *i.e.*, etching, in the post-processing phase [37–39].

The orientation of the build in relation to the printing plate plays a key role in the surface porosity. In particular, a 0° orientation produces a greater degree of porosity than a higher angle. On the contrary, a 45° orientation shows better mechanical features, such as tensile and fatigue properties [24]. In a previous study [40], the effect of the building angle on osteointegration was examined, with the higher contact angles of the SLM surfaces encouraging cell attachment. In comparison with the same gene expression on samples with a 45° orientation, the short-term osseointegration of SLM specimens created at 0° may be expedited.

Electrochemical anodization process permits the generation of an oxide layer with tubes structures on the surface. The setup involved a counter electrode of Ti flat foil and Ti 3D implant immersed in ethylene glycol electrolyte, and NH₄F. A constant voltage was applied. The main technological advantage of anodizing titanium is functionalization of medical implants for better bonding with tissue and enhanced cell growth on the implant [41,42].

The etching process involves the removal of the surface layer of SLM parts by an acid attack. This treatment is widely used to obtain a uniform and clean surface which can be hostile to bacteria but accommodating to host cells. Furthermore, it is attractive due to its simplicity, cost-effectiveness, and potential for large-scale manufacture [43–45].

The key goal of this paper is to combine two different surface modification approaches on 3D-printed Ti6Al4V implants. The combination of building angle effect and post-process treatments creates a specific surface topography that is challenging for biomedical applications.

The building angles chosen for this study were 0° and 45°, following a previous study [40].

Two different post-processing treatments were designed for the modification of the samples taking the original 3D printing features into consideration: anodization and

passivation. In vitro cell experiments were performed to study the effects on cell adhesion, proliferation, and MC3T3-E1 differentiation.

2. Materials and Methods

2.1. Fabrication of the Ti6Al4V Samples

The selective laser melting (SLM) process allows one to set the angle for the laser building strategy in relation to the building plate. Here, the orientations chosen to produce the implant models were 0° and 45°.

Cubical samples (10 × 10 × 10 mm³) were fabricated by SLM using an EOS M290 (EOS, Robert-Stirling-Ring 1, D-82152 Krailling, Germany) with Ti6Al4V (Ti64) inert-gas atomized powder (ARCAM Ti64Al4V powders and EOS Titanium Ti6Al4V). The relevant properties of the used Ti6Al4V powders are reported in Table 1 according to the required datasheets according to ASTM B214, B215, B212, F2924 and F1472 [46–48].

Table 1. SLM Ti64 powders properties and compositions. Data were gathered in accordance with the relevant international ASTM standards.

Particle Size Analysis ¹			Powder Density ²	Chemical Composition ³				
(μm)			(g/cm ³)	(wt %)				
d10	d50	d90		Al	V	O	Fe	Ti
27.79	38.18	54.45	2.31	5.92	4.04	0.13	0.20	Bal.

¹ ASTM B214 and B215 [46]. ² Apparent density, ASTM B212 [47]. ³ ASTM F2924 and F1472 [48]. Bal.—balance.

The SLM samples were produced with the following manufacturing parameters: laser focus diameter 70 μm, laser power 340 W, hatch spacing 40 μm, slice thickness 30 μm, and scanning speed 1250 mm/s.

Specifically, a scanning strategy with alternating angle between layers was used, the variation was set at 67°. Controlled atmosphere was used for the manufacturing to minimize oxygen pick-up to <0.1% with argon gas.

The SLM process requires the building of support structures to guarantee the stability of the samples. The parameters used were the following: laser power 100 W and scanning speed 600 mm/s.

The support structures were removed from the site at the conclusion of the manufacturing process. The standard cleaning methodology used for the samples was sonication in acetone and isopropanol, followed by air drying.

2.2. Post-Processing of the Ti6Al4V Samples

2.2.1. Anodization

Titanium 3D samples were cleaned using ultra-sonication in ethanol to remove surface debris. An oxide layer was fabricated using an electrochemical anodization setup. The setup involved a counter electrode of Ti flat foil and Ti 3D implant immersed in ethylene glycol electrolyte, containing 1% water (*v/v*) and 0.3% NH₄F (*w/v*), maintained at 25 °C, on a magnetic stirrer. A constant voltage of 60 V was applied for 20 min. Post-anodization, the prepared TNT 3D samples were washed with deionized water and dried in cool air.

2.2.2. Etching

The SLM specimens were ultrasonically cleaned in ethanol for 20 min to shake off any trapped powders and clean the samples. Afterwards, the specimens were etched in Kroll reagent (3 mL 48 vol. % HF, 6 mL 70 vol. % HNO₃ and 100 mL water) at room temperature for 10 min. Then, all specimens were cleaned in distilled water and ethanol, ultrasonically and air dried.

2.3. Characterization of the Ti6Al4V Samples

2.3.1. Surface Wettability

Attension Theta Lite optical tensiometer (KSV NIMA Biolin Scientific, Hångpilsgratan 7, 426 77 Västra Frölunda, Sweden) was used to obtain the contact angle measurements.

The measurement was carried out at room temperature and the SLM samples were placed on the bottom flat surface, subsequently a droplet of deionized water (5–10 μL) was pipetted into the centre of the top surface (different building angles were considered). The images of the contact angle were captured following the horizontal plane of the droplet for 30 s after application. To obtain the inner angle between the surface and air/water interface the OneAttension software converts the images to 8-bit grayscale.

2.3.2. Optical Microscopy: Three-Dimensional Surface Reconstruction and Roughness Analysis

Wyko NT1100 3D Optical profilometer (Veeco, One Terminal Drive, Plainview, NY 11803, USA) at $2.5\times$ magnification was used to perform the optical imaging of the SLM samples at different building angles and with different post-processing treatments. The scanning was executed between the maximum and minimum focusing points of the z height of the sample surfaces. A scanning size of $0.92 \times 1.2 \text{ mm}^2$ was selected at the central point of the surface, with a sampling of $1.65 \mu\text{m}$. Vision Veeco Module (Veeco, One Terminal Drive, Plainview, NY 11803, USA) was used to evaluate and analyse the roughness parameter (S_a).

2.3.3. Scanning Electron Microscopy: Surface Topography Analysis

InspectTM environmental SEM (FEI, NSS-II Bldg 4F. 13-34 Kohnan 2-chome. Minato-ku, Tokyo 108-0075, Japan), operating at 20 kV, was used to observe the Ti64Al4V SLM as-built and post-processed specimens. To obtain the topographical imaging, the samples were fixed with double-adhesive carbon tabs at the aluminium stubs. To evaluate the cross-section and examine the surface profile the samples were embedded in cold resin epoxy and then polished.

2.3.4. Statistical Analysis

The statistical tests were carried out to verify if the building angle and the post-processing treatment had any effect on the contact angle and roughness of the samples. Single-factor analysis of variance (ANOVA) tests were performed to confirm any statistical significance within samples and to determine repeatability.

Statistical analysis was conducted at $\alpha = 0.05$ using Minitab 18[®] (MINITAB, Brandon Court Unit E1-E2, Progress Way, Coventry CV3 2TE, UK).

2.4. Biocompatibility Test, and Mineralization Assay

2.4.1. Cell Line

MC3T3-E1 Subclone 4 cells (BS CL 181, IZSLER, A. Bianchi Street, 7/9, 25124 Brescia, Italy) from passage 39 were cultured at 37°C and 5% CO_2 , as previously described [40]. Briefly, the preferential medium to sustain the MC3T3-E1 proliferation is composed of Alpha Minimum Essential Media (α -MEM) with sodium bicarbonate, ribonucleosides, and deoxyribonucleosides (BioConcept, Paradiesrain Street 14, 4123 Allschwil, Switzerland) supplemented with 10% FCS (Euroclone, Figino Street, 20/22, Pero, 20016 Milan, Italy) and 100 units/mL pen/strep (Euroclone, Figino Street, 20/22, Pero, 20016 Milan, Italy). To promote the MC3T3-E1 mineralization the basal medium was enriched by adding $50 \mu\text{g mL}^{-1}$ ascorbic acid (Sigma-Aldrich), 10 mM β -glycerophosphate (Sigma-Aldrich, 3050 Spruce Street, St. Louis, MO 63103, USA), and 100 nM dexamethasone. The mineralization medium was changed every 3 days.

For all assays 5×10^4 cells/cm² were seeded in a proper volume of medium on the titanium substrates and on plastic dish as positive control.

Prior to each in vitro experiment, titanium samples were washed in PBS for 1 h on an orbital shaker, further sterilized in an autoclave at 121 °C for 20 min and put into 12-well plates with a sterile tweezer.

2.4.2. Biocompatibility Tests: Direct and Indirect ATP Cell Viability Assay

CellTiter -Glo 3D Cell Viability (rATP) assay kit (Promega, 2800 Woods Hollow Road, Madison, WI 53711, USA) is an enzymatic assay that utilizes the adenosinotriphosphat (ATP) produced by the cells to convert luciferin into oxyluciferin, which generates a light signal that is proportional to the number of metabolically active cells in culture. A reduced luminescence can be due by either cell death or metabolic quiescence for over-confluence or medium consumption.

For the direct rATP assay, MC3T3-E1 was enzymatically detached and centrifuged at 1300 rpm for 4 min in order to obtain a single cell suspension in fresh medium. The supernatant was removed and MC3T3-E1 were seeded at a cellular density of 5×10^4 cells/cm² on the samples. A concentrated cell suspension was deposited onto each support and incubated for 20 min before filling each well with a proper volume of medium. The same concentration of MC3T3-E1 were seeded on plastic dish as positive control. Cells were maintained at 37 °C in a saturated humidity atmosphere containing 95% air and 5% CO₂. After 24, 48, and 96 h, the substrates were shifted into new culture plates in order to separate the cells that may fall down from the titanium substrates and grow on the plastic dish. Then, residual adherent cells were lysed on the samples using the CellTiter-Glo 3D Reagent and, after 25 min of incubation in the dark, the total volume was transferred into an opaque-walled 96-well plate and the luminescence was recorded using a Tecan Infinite[®] M200 microplate reader (Tecan, Männedorf, Switzerland). Parallely, an ATP standard curve (range of 10 μM to 10 nM) was generated using rATP disodium salt (Promega cat. P1132) to compare the samples luminescence to the standard in order to determine the correct ATP concentration. Hence, the ATP concentration recorded from each sample was calculated and plotted. At each time point, an unpaired *t*-test was conducted on results derived from three different experiments (*n* = 3) to determine if the different surface treatments significantly modified the metabolic activity in comparison with the control samples cultured on plastic dish.

For the indirect rATP assay, titanium supports were placed in a 12-well plate and left to release any potential cytotoxic components into 2 mL of complete α-MEM for 5 days in a humidified incubator at 37 °C and in 5% CO₂ atmosphere. As reference, the same volume of medium was poured in an empty dish and placed in the incubator at the same conditions. The day before the test, MC3T3-E1 were seeded in flat bottom 24-well plates (5×10^4 cells/well). The day after, cell supernatant was removed and replaced by either the titanium sample conditioned medium or control medium. After 24, 48, and 96 h the cells seeded in the 24-well plates were lysed using the CellTiter-Glo 3D Reagent and the rATP assay was performed as described before for the direct test.

2.4.3. Mineralization Evaluation by Osteogenic Gene Expression Analysis

The mineralization process was analysed by collecting the total RNA from the cells adhered to the scaffolds after 30 days of culture. The RNA extraction, RNA retro-transcription into complementary DNA (c-DNA), and the gene expression analysis by quantitative real-time PCR (qPCR) were performed as previously described [40]. The relative quantification of target genes (*Bsp*, *Ocn*, *Opn*, and *Mepe*) was calculated by the $2^{-\Delta\Delta C_t}$ method, using *Gapdh* as housekeeping gene for normalization of the data and the constitutive gene expression of the same markers from MC3T3-E1 cells cultured in basal medium without mineralization as calibrator.

3. Results

3.1. Surface Topography of the Titanium Samples

The scanning electron micrograph analysis shows the surface condition of the samples produced with SLM at various building angles and then processed to modify their surface characteristics (Figure 1).

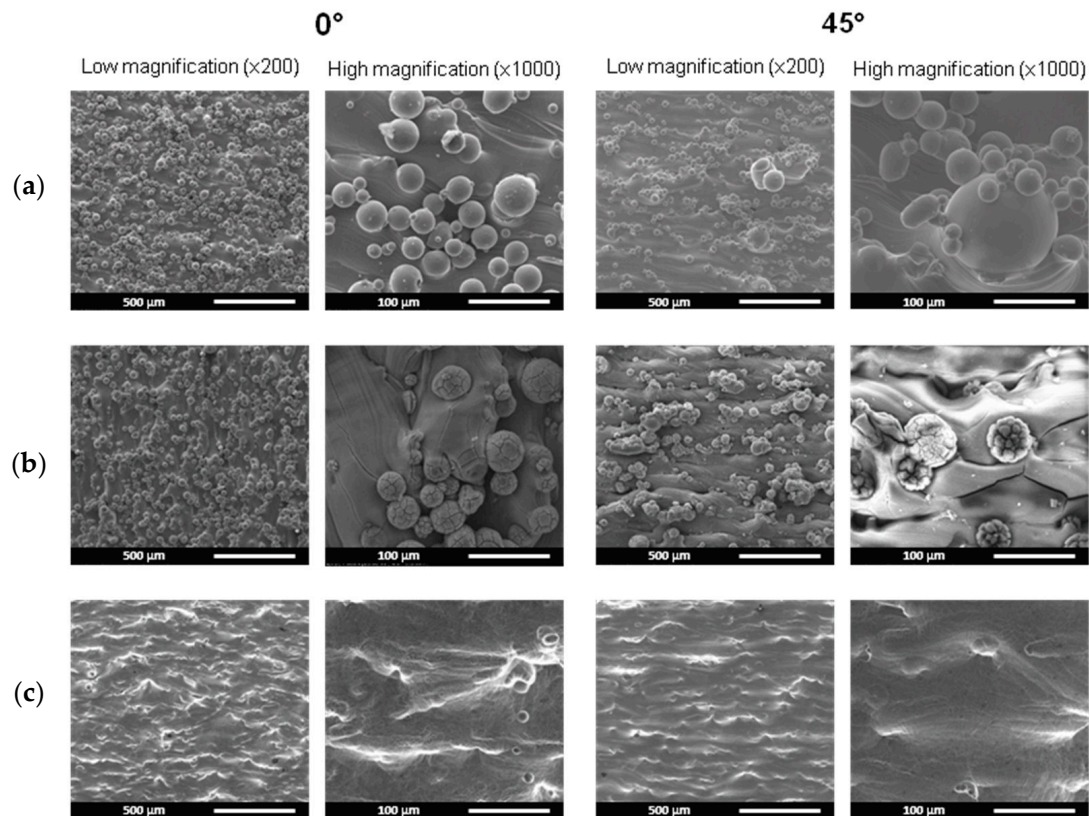


Figure 1. Micrographs illustrating the surface topography of the Ti6Al4V samples manufactured by SLM at 0° and 45°: as-built (a), with post-processing treatments anodization (b) and etching (c).

A distinct distribution of spherical, partially melted powder particles is observed in the as-built samples. Particularly for samples with a 0° building angle, the particles are uniformly distributed over the surface; however, when the building angle is increased to 45°, the particles have a diameter comparable to the 0° sample, ranging from 30–50 μm, but have a less homogeneous distribution, with the formation of clusters on the order of 130 μm in diameter (Figure 1).

The anodization treatment causes no considerable morphological alterations to the sample surface at the 0° building angle, in fact the same uniformity of particles distribution is observed. The 45° samples, on the other hand, exhibit considerable morphological alterations. Cracks appear on the spherical surface of the particles and the number and dimension of the clusters increase.

However, the significant surface alteration is due to the etching treatment. The acid attack totally smooths the surface of the specimens, regardless of the building angle. Particles are almost absent, with only roughness ridges and a few craters visible, probably caused by the detachment of clusters or particles with bigger diameters.

The effect of post-processing treatments on the surface is highlighted by the contact angle (CA) and roughness values. Notably, the CA of the as-built surface samples is comparable between the two different building angles but has a significant decrease with the post-processing treatments (Table 2). The hydrophilic characteristics of the metal samples are somewhat impacted by anodization and the etching procedures; however,

most notable is the combination between building angle and post-processing treatments. In fact, the etching treatment has no such significant effect on the samples with building angle at 45°, but on the samples produced at 0° the CA is significantly lower.

Table 2. CA measurements and statistical evaluation of the as-built, anodized and etched samples.

Angle SLM	Mean Value [°]			p-Value
	As-Built	Anodized	Etched	
0°	129.64 ± 5.32	75.48 ± 5.31	70.64 ± 5.70	0.003
45°	120.91 ± 2.32	38.8 ± 24.1	108.48 ± 0.993	0.018

In contrast, the anodizing treatment is more critical, since it dramatically modifies the surface performance of the specimen with a building angle of 45° in relation to 0°, but with values that deviate too much from the average (Figure 2).

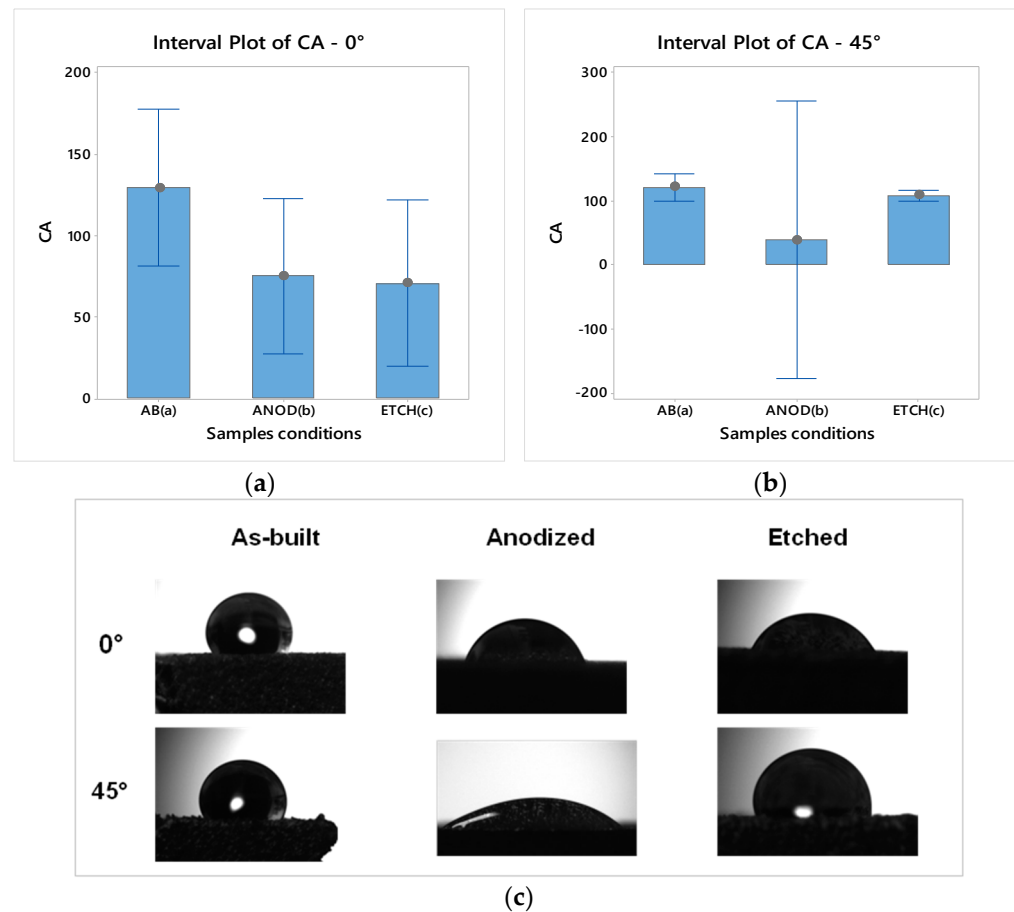


Figure 2. CA measurements for the samples: (a) 0° building angle individual samples; (b) 45° building angle individual samples; (c) images of the water droplets on the top surfaces at different building angles and treatments.

The one-way ANOVA test performed on the CA measurements of the samples reveals that the aspect is considered statistically significant (Table 2). It is therefore significant to note that, in this work, altering the construction angle is not shown to have a substantial impact on the hydrophobicity of the surfaces, however the selection of the post-processing treatment is crucial.

The surface roughness Sa is measured to evaluate the sample surface finishing in relation to the manufacturing operations. For each measurement, three were used and results were elaborated with one-way ANOVA test. The results demonstrate the influence

of the building strategy, in particular the building angle, and post-processing treatments. The Sa roughness increases with increasing angle, despite being comparable in magnitude. This difference is consistent due to the presence of clusters and the irregular dispersion of particles as observed in the scanning electron micrograph.

The roughness is greatly reduced by the anodizing procedure, which also equalizes the differences between 0° and 45° samples, making the values comparable to the micrometre. The etching procedure significantly reduces surface roughness. The Sa values demonstrate the surface’s full smoothness, as shown in the micrographs. Moreover, there are no appreciable differences between the samples with various building angle.

The production strategy of the samples has a low impact on roughness if they are subjected to post-processing treatments such as anodization or etching. Statistical significance and value trends are shown in Table 3 and in Figure 3.

Table 3. Sa measurements and statistical evaluation of the as-built, anodized and etched samples.

Angle SLM	Mean Value [°]			p-Value
	As-Built	Anodized	Etched	
0°	17.84 ± 4.76	6.29 ± 0.399	2.307 ± 0.326	0.001
45°	20.40 ± 5.02	6.35 ± 2.71	2.200 ± 0.416	0.001

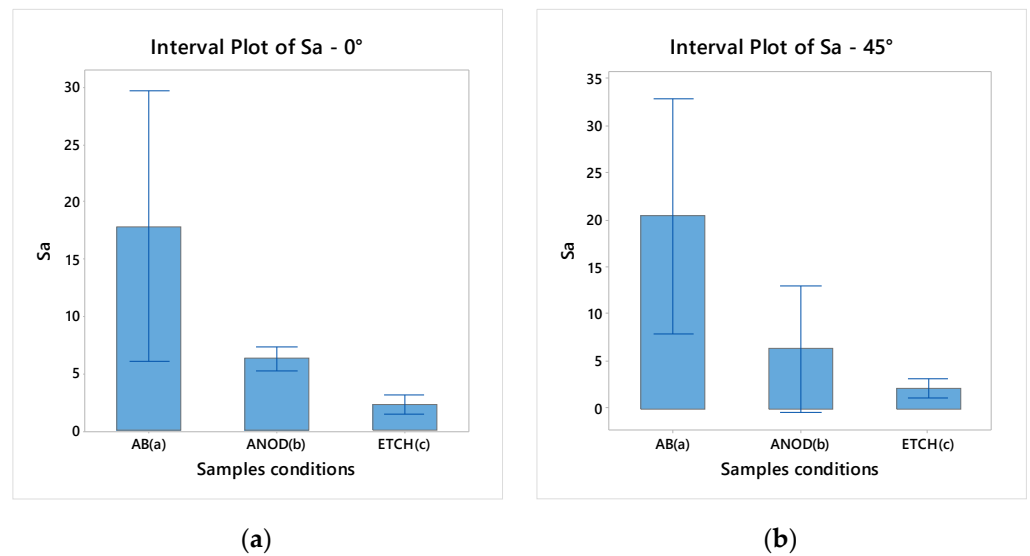


Figure 3. Sa measurements for the samples: (a) 0° building angle individual samples; (b) 45° building angle individual samples.

The SEM metallographic cross-section samples show the surface profile of the top surfaces of the different printed parts (Figure 4): as-built, anodized and etched.

The profiles along the cross-sections of the samples reveal a varied trend at different building angles and post-processing treatments. The as-built samples exhibit surface features that were created as a result of the powder on the top layer partially melting. In particular, as the angle increases so does the superficial structure in number and dimensions. The surface aspect is highly dependent on post-processing treatment. The anodized samples show surfaces with protruding structures that became more severe when the building angle increases and which show an irregular and roughened profile. The partial melting particles are still present but the etched samples show smoothed surfaces without significant differences. This is due to the building angle and lack of residual particles typical of an SLM manufacturing process.

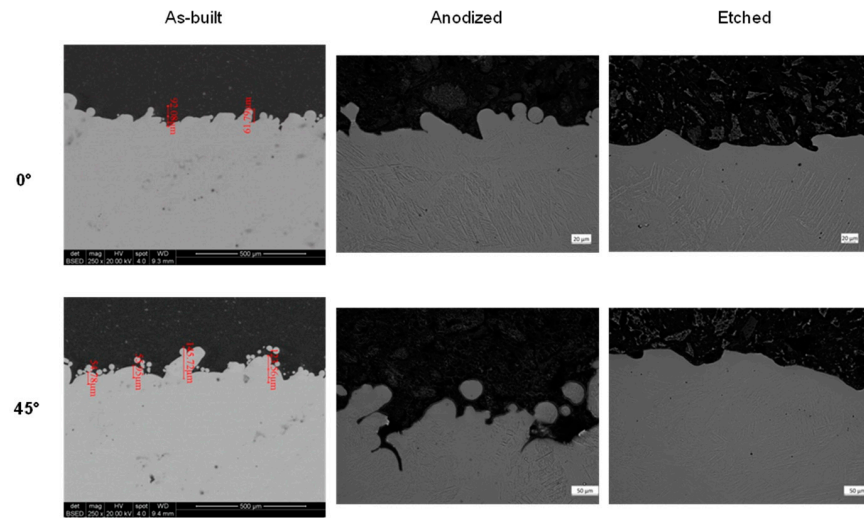


Figure 4. Micrographs illustrating the surface profile of the cross-sections of the samples built at different building angles and with different treatments.

3.2. Biocompatibility of Titanium Scaffolds

3.2.1. Direct rATP Assay

The application of biocompatible materials is essential to promote and sustain the metabolic activities of the seeded cells. In particular, the substrate chosen should guarantee the cellular survival and the metabolism. The environment, the so called “biological niche”, is full of stimuli for cellular growth, differentiation and maturation. Cells in an unfavourable environment for replication arrest their cell cycle into a quiescent phase even as they remain viable. rATP assay detects the ATP produced by the cells and allows one to analyse the biocompatibility of a material while studying the metabolic activity of the cells cultured on it. MC3T3-E1 cells were seeded onto as-built, anodized and etched (0° and 45°) SLM scaffolds and analysed after 24, 48, and 96 h in culture. Figure 5 shows ATP (µM) concentrations at different time points of MC3T3-E1 cultured onto plastic, as internal control, and on each scaffold typology.

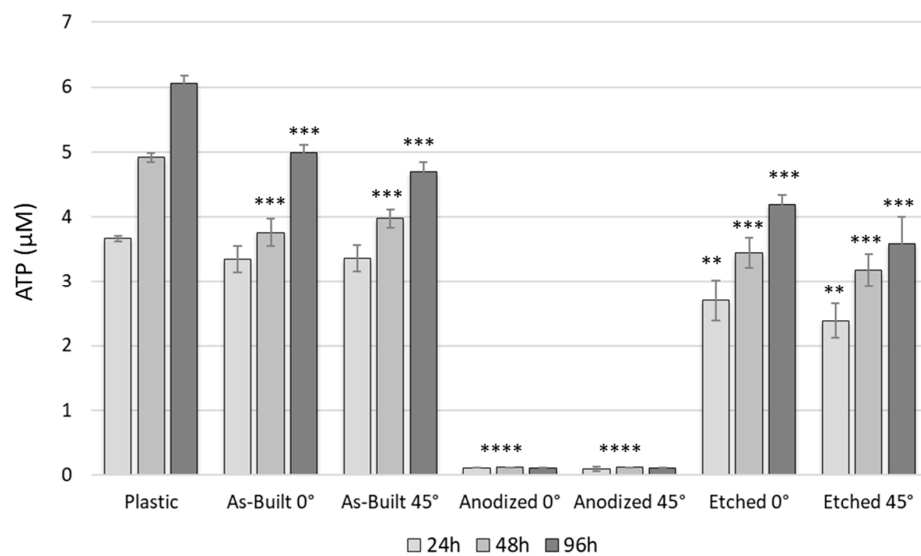


Figure 5. ATP (µM) concentrations of MC3T3-E1 cells cultured on titanium as-built, anodized and etched 0° and 45° SLM scaffolds and on a plastic dish after 24 h, 48 h, and 96 h. Unpaired *t*-test was applied to discriminate differences between MC3T3-E1 cultured on a plastic dish and on each scaffold considering a statistically significant value of $p < 0.05$ (** $p < 0.01$, *** $p < 0.001$, **** $p < 0.0001$).

A positive growth trend of proliferation is observed for MC3T3-E1 on the plastic well plate, unlike cells grown on the titanium substrates that show a variable behaviour. Cells on the SLM as-built scaffolds confirmed the biocompatibility already shown previously [40]. The cellular viability of MC3T3-E1 on etched SLM is reduced for both angles of fabrication in comparison with the plastic dish, with significant differences. By contrast, the anodized samples show a strong statistical significant decrease in metabolic activity, evident as early as 24 h after the cells seeding (p value < 0.0001).

3.2.2. Indirect rATP Assay

In order to understand if the absence of cellular metabolic activity observed for the anodized samples is related to a bio-incompatibility of the material or to a cellular adhesion problem that may have caused the loss of all the cells on the substrates, an indirect rATP assay was performed. Specifically, the analysis included the ATP concentration derived from MC3T3-E1 cultured in conditioned medium (medium collected from dishes containing each typology of titanium substrate for five days in an incubator), and in control medium (medium put in an empty well and kept at the same conditions) as experimental positive control. With this kind of test, it is possible to bypass any differences in terms of cell adhesion potential of each substrate and consider only the biocompatibility of the material. Figure 6 shows the result of the indirect rATP assay at three time points (24, 48, 96 h). Medium collected from anodized substrates results in drastically high levels of cytotoxicity as early as 24 h, showing no cellular survival (p value < 0.0001). By contrast, medium collected from other titanium scaffolds shows a biocompatible potential: the cell viability trend is comparable to the control medium with no statistical significant differences between angles of fabrication or treatment.

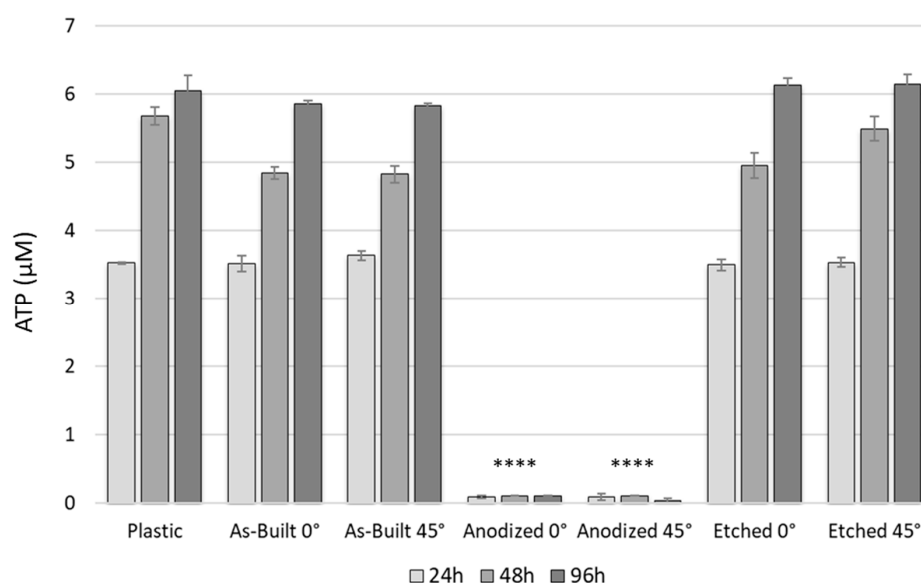


Figure 6. ATP (μM) concentrations of MC3T3-E1 cells cultured in conditioned and in control medium at different time points (24 h, 48 h, and 96 h). Unpaired t -test was applied to discriminate differences between MC3T3-E1 cultured on a plastic dish and on each scaffold considering a statistically significant value of $p < 0.05$ (**** $p < 0.0001$).

3.2.3. Osteogenic Differentiation and Mineralization on Titanium Scaffolds

The biological characterization of the titanium supports described in this work was deepened only for the etching treatment, as the anodizing samples were not found to be biocompatible. In particular, the mineralization potentials of the etched titanium scaffolds at the 0° and 45° angles of fabrication were investigated in comparison with previously validated [40] as-built scaffolds and plastic controls. To analyse the osteogenic differentiation of a pre-osteoblastic MC3T3-E1 cell line cultured for 30 days in the mineralization medium,

total RNA was collected from cells adhered on each substrate. Then, gene expression of several markers involved in osteogenesis (*Mepe*, *Bsp*, *Opn*, and *Ocn*) was determined by performing quantitative RT-PCR (qPCR)

The relative quantification (RQ) of the osteogenic target genes was calculated by the $2^{-\Delta\Delta C_t}$ method, using the constitutive gene expression of the same markers obtained from cells cultured in basal medium as calibrator (RQ calibrator = 1). Figure 7 shows the RQ results as mean of three different experiments ($n = 3$) for plastic dish (positive control) and as-built and etched scaffolds (both 0° and 45° angles of fabrication). All the genes tested were induced in all samples in comparison with the basal level expression (RQ = 1), indicating that a positive mineralization process occurred. No statistically significant differences are detected for *Mepe* and *Bsp* gene expression between control and titanium substrates. An opposite trend is observed for the *Opn* and *Ocn* gene expression, these markers show statistically significant dissimilar expression in cells collected from titanium scaffolds in comparison with those collected from a plastic dish.

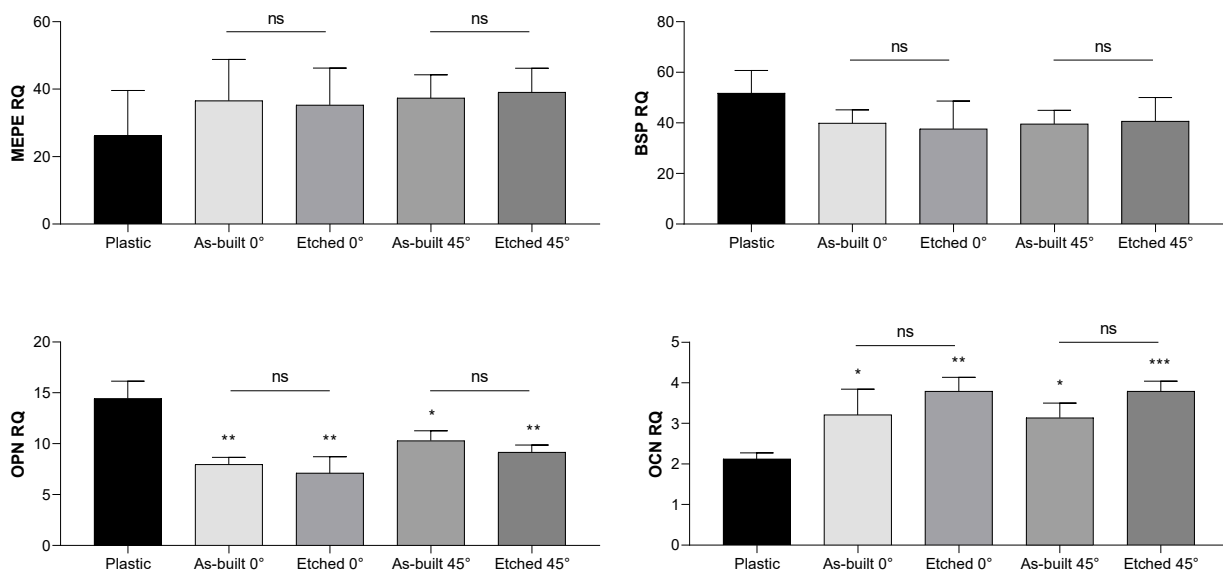


Figure 7. Gene expression evaluation of MC3T3-E1 cells cultured in mineralization medium after 30 days on titanium as-built and etched (0° and 45°) SLM scaffolds and on a plastic well plate. Unpaired *t*-test was applied to discriminate differences between plastic dish and each scaffold considering a statistically significant value of $p < 0.05$ (* $p < 0.05$, ** $p < 0.01$, *** $p < 0.001$). Unpaired *t*-test was used also to compare as-built substrates and relative etched scaffolds (“ns” indicates not significant, $p > 0.05$).

Specifically, the *Ocn* gene expressions on the as-built and etched substrates show a significant increase with respect to the control group, which is more evident for the etched substrates with a higher angle of fabrication (p -value < 0.001). On the contrary, the *Opn* gene expression on the scaffold groups is significantly reduced in comparison with the control group (p -value < 0.05). Since it is known in the literature that *Ocn* is a late-stage marker of osteoblastic differentiation, typical of mature osteoblasts, whereas *Opn* is commonly defined as early markers of osteogenic differentiation [49], the observed gene expression trend reflects and confirms an acceleration in the mineralization process of the MC3T3-E1 cells grown on titanium scaffolds versus cells cultured in plastic well [40]. Finally, the statistical analysis comparing the gene expression of the cells grown on the as-built substrates and on those treated does not show any significant difference in terms of mineralization potential for any angles of fabrication.

4. Discussion

Surface modification of a scaffold for biological application can be achieved using different techniques and approaches [50–52]. The manufacturing process analysed in this paper includes some critical aspects because a particular production technology, the SLM technique, is integrated with two different post-processing treatments, anodization and passivation, i.e., acid etching. All the powder bed fusion techniques result in complex thermal properties and significant temperature gradients that make the surface conditions of the products difficult to optimize, and add variables to the process. Due to this, it is challenging to guarantee the uniformity of the product characteristics and the repeatability of the whole process, aspects that are essential when adopting metal additive manufacturing methods as industrial processes.

The transformation of the microstructure incurred by the combination of the SLM process parameters—specifically the building angle, followed by chemical and physical modification with anodization and etching in the post-processing phase—generates relevant outcomes [39].

The surface microstructure of the as-built SLM samples shows how the used building angles had an impact on their attributes. In fact, several studies have shown how, in a metal part, mechanical and chemical surface properties can be significantly altered by the building angle of a melting process [30,37]. However, the key to enhancing a product's surface characteristics for biomedical applications is adding post-process treatments. The two processes that are most frequently used to modify AM metal implants are anodization and acid etching. To determine the relationship between the manufacturing process and the post-process treatments, two building angles (0° and 45°) were studied according to previous research [40].

The surfaces of the SLM as-built samples, at two distinct building angles, appear to be macroscopically identical when compared with each other, and both show the presence of partially melted particles seen across the whole surface area of the top faces. According to [24], the surfaces of the parts with a building angle at 0° particularly exhibit equally distributed particles, whereas the surfaces of the parts with a building angle at 45° exhibit less uniform distribution and the presence of larger-sized agglomerations of particles (Figure 1). This surface condition is supported by the measurement of roughness; in fact, the S_a value of the parts with a 45° building angle is higher compared with the other samples with a lower building angle (Table 3). For both the building angles, the CA measurements highlight the hydrophobicity of the SLM as-built samples, and the resulting values are comparable (Table 2). Due to these similarities, there has not been any significant difference in the viability values of MC3T3-E1 cells between the SLM as-built samples for either building angle (Figure 5). The biocompatibility previously demonstrated [40] was verified by cells on the SLM as-built scaffolds.

The impact of surface modification on biological performance is most noticeable on samples that have been treated. In general, similar amounts of cellular metabolic activity are evaluated for SLM as-built and etched samples, but for the anodized scaffolds, an undeniable contrast between the plastic control and the cells metabolic activity is seen (Figure 6).

The anodized samples have an adequate uniform particle distribution for the 0° samples, but when the angle is increased to 45° , the particle distribution becomes random with the formation of clusters and the appearance of cracks on the surface of the particles (Figure 1). This is also demonstrated by the hydrophobicity, which is significantly reduced compared with the as-built samples, notably for the 45° angle (Table 2). Compared with the as-built samples, the roughness is comparable for both building angles and is decreased (Table 3).

In contrast, the etched scaffolds exhibit a morphological surface that is smooth, with roughness and hydrophobicity values that are lower when compared with anodized samples built at 0° but higher when built at 45° (Table 2). According to [39], there is a need for

an ideal implant surface to be smooth to avoid bacterial proliferation, but at the same time have a uniform micro-structure to promote cell adhesion.

The application of post-processing treatments is not affected by the building angle of the specimen. In fact, it is not possible to find a direct relation between build angle and the other parameters used to describe the surface, mainly because the application of post-processing treatments creates a strong alteration of the surface that makes the effect of the building angle irrelevant. Roughness decreases with treatments, but when evaluating the values in relation to the build angles, it has an opposite trend depending on the treatment applied (Figure 3). Additionally, the CA values have no significant relation with the building angle (Figure 2). For a more functional evaluation of surface performance for biomedical applications, cell viability studies are necessary. Titanium substrate biocompatibility has been analysed using an rATP assay kit that measures the number of metabolically active and viable cells in a culture. The rATP test has been performed in a direct way (cells were seeded directly on the sterilized titanium substrates) and in an indirect way (autoclaved titanium substrates were placed in medium for five days, then the conditioned medium was used to grow cells). In both conditions, the results of the rATP assay showed a robust decrease of cellular viability for the anodized samples. In fact, no living cells were detected in the culture after 24 h (Figures 5 and 6). Conversely, biocompatibility of the as-built specimens and specimens after acid etching treatment was confirmed (Figures 5 and 6). Taking into account the high cellular mortality also showed with the indirect rATP assay, it is plausible that the cellular death is not related to an adhesion problem with the scaffold but to some cytotoxic agents probably derived from the post-processing of the samples, resistant to the autoclaving, that are released in the medium culture from the anodized substrates' surface. The post-processing for the anodized titanium 3D samples consists of the fabrication of an oxide layer using an electrochemical anodization setup composed of a counter electrode of Ti flat foil and Ti 3D implant immersed in ethylene glycol electrolyte, containing 1% water and 0.3% NH₄F. Further studies are needed to identify which reagent in this treatment might be toxic.

Finally, it is shown that there is an acceleration in the mineralization process of the MC3T3-E1 cells grown on titanium scaffolds versus cells cultured in plastic well (Figure 7). At the present time it is difficult to properly compare the approaches utilised for the surface treatment of 3D printed implants intended to promote cell adhesion and mineralization [53]. The chemical and physical characteristics of the surfaces also play a significant role in maintaining the viability of the osteoblasts. Many aspects of these interactions require more investigation to resolve areas of uncertainty on the interaction between the treated surfaces and the cells. To completely comprehend these linkages, research needs to focus on diverse design aspects using various combinations of manufacturing processes and surface treatments.

5. Conclusions

In this paper, the examination of additive manufacturing properties on the biocompatibility of Ti6Al4V parts is reported. The porosity and surface conditions of an implant can be tuned in order to facilitate and promote osseointegration. This is especially true of parts that can be produced by utilizing the PBF process and the SLM technique. The discontinuous melting of the powder during the building process, which results in uncontrolled and partially melted particles on the surface and conditions the surface area of the scaffold, is one of the main drawbacks of these methods. As a result of these aspects, a lot of research has focused on changing the process parameters and including post-process treatments. The examined solutions focus on changing the building angle during SLM operations (0° and 45°) and on the use of two treatments, anodizing and acid etching, to regulate and customize the surface properties of the metal parts. Due to the initially identical surface topography, it was discovered that the building angle has little effect on the trends of cell attachment and differentiation ($p > 0.05$). The key finding of this study is based on osteoblast metabolic activity and differentiation data, which show

a clear distinction between samples after acid etching and anodization. In particular, it was discovered that SLM as-built samples are more biocompatible than post-processed ones. In comparison with the control on plastic, the cell viability on etched SLM is lower ($p < 0.05$; Figure 5). The metabolic activity on the anodized samples significantly decreased, leading to substantial levels of cytotoxicity with no cellular survival as a result (p value < 0.0001 ; Figures 5 and 6). A successful mineralization process took place on the as-built and etched scaffolds. In particular, when comparing cells cultured in plastic wells with cells grown on titanium scaffolds, the observed gene expression trend reflects and validates an acceleration of the mineralization process, for any manufacturing angle (Figure 7). This issue needs to be examined in more detail in order to optimize the procedure and produce results that are more targeted to biological applications. In fact, it could be seen as a benefit for the osseointegration of intricate components in a custom implant. Additionally, mineralization can be advantageous for the majority of orthopaedic implants, but it could be detrimental for short-term removable components. The study of the findings of this research on bacterial adhesion [54], a crucial factor for this application, will be taken into account in future investigations.

In conclusion, in relation to the SLM design technique utilized in production, post-processing treatments have a significant impact on the characteristics of 3D printed implants.

Author Contributions: Conceptualization, P.G. and R.M.F.; methodology, P.G., K.Z.-H. and R.M.F.; formal analysis, P.G.; investigation, P.G., R.M.F. and K.Z.-H.; resources, R.M.F., K.Z.-H., S.G. and E.C.; data curation, R.R. and R.M.F.; writing—original draft preparation, R.R., P.G. and R.M.F.; writing—review and editing, P.G., K.Z.-H., R.M.F., S.G. and E.C.; supervision, E.C. and S.G.; project administration, E.C.; funding acquisition, P.G. and E.C. All authors have read and agreed to the published version of the manuscript.

Funding: This research was funded by the Israel–Italy “Joint Innovation Program” for Research and Development Cooperation in Industrial, Scientific and Technological fields in R&D (Industrial Track, Grant Name: OPTIMIB) founded by the Italian Ministry of Foreign Affairs and Israeli Innovation Authority. CUP D16C18001710006.

Data Availability Statement: Data available on request due to restrictions eg privacy or ethical. The data presented in this study are available on request from the corresponding author. The data are not publicly available due to the privacy policy of the Institutions upon PhDs project prior to thesis final defence.

Acknowledgments: The authors would like to acknowledge the support of the KANFIT3D AM company (8 Hamerkava Street, Tziporit Industrial Zone, Nof Hagalil 1789064, Israel) for the production of the SLM samples.

Conflicts of Interest: The authors declare no conflict of interest.

References

1. Velu, R.; Calais, T.; Jayakumar, A.; Raspall, F. A Comprehensive Review on Bio-Nanomaterials for Medical Implants and Feasibility Studies on Fabrication of Such Implants by Additive Manufacturing Technique. *Materials* **2020**, *13*, 92. [[CrossRef](#)] [[PubMed](#)]
2. Ginestra, P.; Ceretti, E.; Fiorentino, A. Potential of modeling and simulations of bioengineered devices: Endoprostheses, prostheses and orthoses. *Proc. Inst. Mech. Eng. Part H J. Eng. Med.* **2016**, *230*, 607–638. [[CrossRef](#)] [[PubMed](#)]
3. Bayata, F.; Yildiz, C. The effects of design parameters on mechanical failure of Ti-6Al-4V implants using finite element analysis. *Eng. Fail. Anal.* **2020**, *110*, 104445. [[CrossRef](#)]
4. Doliveux, S.; Jamjoom, F.Z.; Nadra, M.; Gallucci, G.O.; Hamilton, A. Fabrication technique for a custom implant emergence profile on 3D printed casts. *J. Prosthet. Dent.* **2020**, *123*, 571–575. [[CrossRef](#)] [[PubMed](#)]
5. Angelats, D.; Ginestra, P. Cell Bioprinting: The 3D-Bioplotter™ Case. *Materials* **2019**, *12*, 4005. [[CrossRef](#)] [[PubMed](#)]
6. Lowther, M.; Cox, S.C.; Davey, A.; Hussain, A.; Ginestra, P.; Carter, L.; Eisenstein, N.; Grover, L.M.; Cox, S.C. Clinical, industrial, and research perspectives on powder bed fusion additively manufactured metal implants. *Addit. Manuf.* **2019**, *28*, 565–584. [[CrossRef](#)]
7. Tilton, M.; Lewis, G.S.; Wee, H.B.; Armstrong, A.; Hast, M.W.; Manogharan, G. Additive manufacturing of fracture fixation implants: Design, material characterization, biomechanical modeling and experimentation. *Addit. Manuf.* **2020**, *33*, 101137. [[CrossRef](#)]

8. Li, C.-H.; Wu, C.-H.; Lin, C.-L. Design of a patient-specific mandible reconstruction implant with dental prosthesis for metal 3D printing using integrated weighted topology optimization and finite element analysis. *J. Mech. Behav. Biomed. Mater.* **2020**, *105*, 103700. [[CrossRef](#)]
9. Ni, J.; Ling, H.; Zhang, S.; Wang, Z.; Peng, Z.; Benyshek, C.; Zan, R.; Miri, A.K.; Li, Z.; Zhang, X.; et al. Three-dimensional printing of metals for biomedical applications. *Mater. Today Bio* **2019**, *3*, 100024. [[CrossRef](#)]
10. Nirish, M.; Rajendra, R. Suitability of metal additive manufacturing processes for part topology optimization—A comparative study. *Mater. Today Proc.* **2020**, *27*, 1601–1607. [[CrossRef](#)]
11. Zhao, D.; Han, C.; Li, Y.; Li, J.; Zhou, K.; Wei, Q.; Liu, J.; Shi, Y. Improvement on mechanical properties and corrosion resistance of titanium-tantalum alloys in-situ fabricated via selective laser melting. *J. Alloy. Compd.* **2019**, *804*, 288–298, ISSN 0925-8388. [[CrossRef](#)]
12. Makhetha, W.M.I.; Becker, T.H.; Sacks, N. Post-Processing Framework for As-Built LPBF Ti-6Al-4V Parts Towards Meeting Industry Functional Requirements. *JOM* **2022**, *74*, 764–776. [[CrossRef](#)]
13. Grover, T.; Pandey, A.; Kumari, S.T.; Awasthi, A.; Singh, B.; Dixit, P.; Singhal, P.; Saxena, K. Role of titanium in bio implants and additive manufacturing: An overview. *Mater. Today Proc.* **2020**, *26*, 3071–3080. [[CrossRef](#)]
14. Zhang, L.-C.; Chen, L.-Y. A Review on Biomedical Titanium Alloys: Recent Progress and Prospect. *Adv. Eng. Mater.* **2019**, *21*, 1801215. [[CrossRef](#)]
15. Khorasani, A.M.; Goldberg, M.; Doeven, E.H.; Littlefair, G. Titanium in Biomedical Applications—Properties and Fabrication: A Review. *J. Biomater. Tissue Eng.* **2015**, *5*, 593–619. [[CrossRef](#)]
16. Sidhu, S.S.; Gepreel, M.A.-H.; Bahraminasab, M. Advances in titanium bio-implants: Alloy design, surface engineering and manufacturing processes. *J. Mater. Res.* **2022**, *37*, 2487–2490. [[CrossRef](#)]
17. Balasubramanian Gayathri, Y.K.; Kumar, R.L.; Ramalingam, V.V.; Priyadharshini, G.S.; Kumar, K.S.; Prabhu, T.R. Additive Manufacturing of Ti-6Al-4V alloy for Biomedical Applications. *J. Bio Tribo. Corros.* **2022**, *8*, 98. [[CrossRef](#)]
18. Murr, L.E. Metallurgy principles applied to powder bed fusion 3D printing/additive manufacturing of personalized and optimized metal and alloy biomedical implants: An overview. *J. Mater. Res. Technol.* **2020**, *9*, 1087–1103. [[CrossRef](#)]
19. Bhanupratap, G.; Deepak, S.; Rupesh, G.; Ravi, B. Ti6Al4V scaffolds fabricated by laser powder bed fusion with hybrid volumetric energy density. *Rapid Prototyp. J.* **2023**, *29*, 67–79, ISSN 1355-2546.
20. Aufa, A.N.; Zaki Hassan, M.; Ismail, Z. Recent advances in Ti-6Al-4V additively manufactured by selective laser melting for biomedical implants: Prospect development. *J. Alloy. Compd.* **2022**, *896*, 163072, ISSN 0925-8388. [[CrossRef](#)]
21. Buhairi, M.A.; Foudzi, F.M.; Jamhari, F.I.; Sulong, A.B.; Radzuan, N.A.M.; Muhamad, N.; Mohamed, I.F.; Azman, A.H.; Harun, W.S.W.; Al-Furjan, M.S.H. Review on volumetric energy density: Influence on morphology and mechanical properties of Ti6Al4V manufactured via laser powder bed fusion. *Prog. Addit. Manuf.* **2022**. [[CrossRef](#)]
22. Eskandari, H.; Lashgari, H.R.; Zangeneh, S.; Kong, C.; Ye, L.; Eizadjou, M.; Wang, H. Microstructural characterization and mechanical properties of SLM-printed Ti-6Al-4V alloy: Effect of build orientation. *JMatR* **2022**, *37*, 2645. [[CrossRef](#)]
23. Krakhmalev, P.; Fredriksson, G.; Yadroitsava, I.; Kazantseva, N.; Du Plessis, A.; Yadroitsev, I. Deformation behavior and microstructure of Ti6Al4V manufactured by SLM. *Phys. Procedia* **2016**, *83*, 778–788. [[CrossRef](#)]
24. NEW Mukalay, T.A.; Johan Trimble, J.A.; Mpofu, K.; Muvunzi, R. A systematic review of process uncertainty in Ti6Al4V-selective laser melting. *CIRP J. Manuf. Sci. Technol.* **2022**, *36*, 185–212, ISSN 1755-5817. [[CrossRef](#)]
25. Carter, L.N.; Villapún, V.M.; Grover, L.; Cox, S.C. Exploring the duality of powder adhesion and underlying surface roughness in laser powder bed fusion processed Ti-6Al-4V. *J. Manuf. Process.* **2022**, *81*, 14–26, ISSN 1526-6125. [[CrossRef](#)]
26. Dos Santos, L.C.P.; Malheiros, F.C.; Guarato, A.Z. Surface parameters of as-built additive manufactured metal for intraosseous dental implants. *J. Prosthet. Dent.* **2020**, *124*, 217–222. [[CrossRef](#)]
27. Rodriguez, G.M.; Bowen, J.; Zelzer, M.; Stamboulis, A. Selective modification of Ti6Al4V surfaces for biomedical applications. *RSC Adv.* **2020**, *10*, 17642–17652. [[CrossRef](#)]
28. Zhou, W.; Peng, X.; Ma, Y.; Hu, Y.; Wu, Y.; Lan, F.; Weir, M.D.; Li, M.; Ren, B.; Oates, T.W.; et al. Two-staged time-dependent materials for the prevention of implant-related infections. *Acta Biomater.* **2020**, *101*, 128–140. [[CrossRef](#)]
29. Sarker, A.; Tran, N.; Rifai, A.; Brandt, M.; A Tran, P.; Leary, M.; Fox, K.; Williams, R. Rational design of additively manufactured Ti6Al4V implants to control Staphylococcus aureus biofilm formation. *Materialia* **2019**, *5*, 100250. [[CrossRef](#)]
30. Xie, K.; Guo, Y.; Zhao, S.; Wang, L.; Wu, J.; Tan, J.; Yang, Y.; Wu, W.; Jiang, W.; Hao, Y. Partially Melted Ti6Al4V Particles Increase Bacterial Adhesion and Inhibit Osteogenic Activity on 3D-printed Implants: An In Vitro Study. *Clin. Orthop. Relat. Res.* **2019**, *477*, 2772–2782. [[CrossRef](#)]
31. Ren, B.; Wan, Y.; Liu, C.; Wang, H.; Yu, M.; Zhang, X.; Huang, Y. Improved osseointegration of 3D printed Ti-6Al-4V implant with a hierarchical micro/nano surface topography: An in vitro and in vivo study. *Mat. Sci. Eng. C-Mater.* **2021**, *118*, 111505. [[CrossRef](#)] [[PubMed](#)]
32. Ginestra, P.; Fiorentino, A.; Ceretti, E. Micro-structuring of Titanium Collectors by Laser Ablation Technique: A Promising Approach to Produce Micro-patterned Scaffolds for Tissue Engineering Applications. *Procedia CIRP* **2017**, *65*, 19–24. [[CrossRef](#)]
33. Ginestra, P.; Pandini, S.; Fiorentino, A.; Benzoni, P.; Dell’Era, P.; Ceretti, E. Microstructured scaffold for guided cellular orientation: Poly(ϵ -caprolactone) electrospinning on laser ablated titanium collector. *CIRP J. Manuf. Sci. Technol.* **2017**, *19*, 147–157. [[CrossRef](#)]
34. Malik, A.; Rouf, S.; Ul Haq, M.I.; Raina, A.; Valerga Puerta, A.P.; Sagbas, B.; Ruggiero, A. Tribo-corrosive behavior of additive manufactured parts for orthopaedic applications. *J. Orthop.* **2022**, *34*, 49–60. [[CrossRef](#)] [[PubMed](#)]

35. Erwin, N.; Sur, D.; Basim, G.B. Remediation of machining medium effect on biocompatibility of titanium-based dental implants by chemical mechanical nano-structuring. *J. Mater. Res.* **2022**, *37*, 2686–2697. [[CrossRef](#)]
36. Dwivedi, S.; Dixit, A.R.; Das, A.K.; Adamczuk, K. Additive texturing of metallic implant surfaces for improved wetting and biotribological performance. *J. Mater. Res. Technol.* **2022**, *20*, 2650–2667, ISSN 2238-7854. [[CrossRef](#)]
37. Zhang, D.J.; Zhao, C.; Sheng, R.; Lin, K.; Wang, X.; Zhang, S. Construction of a Hierarchical Micro-/Submicro-/Nanostructured 3D-Printed Ti6Al4V Surface Feature to Promote Osteogenesis: Involvement of Sema7A through the ITGB1/FAK/ERK Signaling Pathway. *ACS Appl. Mater. Interfaces* **2022**, *14*, 30571–30581. [[CrossRef](#)]
38. Wang, H.; Liu, J.; Wang, C.; Shen, S.C.; Wang, X.; Lin, K. The synergistic effect of 3D-printed microscale roughness surface and nanoscale feature on enhancing osteogenic differentiation and rapid osseointegration. *J. Mater. Sci. Technol.* **2021**, *63*, 18–26, ISSN 1005-0302. [[CrossRef](#)]
39. Stepanovska, J.; Matejka, R.; Otahal, M.; Rosina, J.; Bacakova, L. The Effect of Various Surface Treatments of Ti6Al4V on the Growth and Osteogenic Differentiation of Adipose Tissue-Derived Stem Cells. *Coatings* **2020**, *10*, 762. [[CrossRef](#)]
40. Ginestra, P.; Ferraro, R.M.; Zohar-Hauber, K.; Abeni, A.; Giliani, S.; Ceretti, E. Selective Laser Melting and Electron Beam Melting of Ti6Al4V for Orthopedic Applications: A Comparative Study on the Applied Building Direction. *Materials* **2020**, *13*, 5584. [[CrossRef](#)]
41. Izmir, M.; Ercan, B. Anodization of titanium alloys for orthopedic applications. *Front. Chem. Sci. Eng.* **2019**, *13*, 28–45. [[CrossRef](#)]
42. Manjiah, M.; Laubscher, R.F. Effect of anodizing on surface integrity of Grade 4 titanium for biomedical applications. *Surf. Coat. Technol.* **2017**, *310*, 263–272, ISSN 0257-8972. [[CrossRef](#)]
43. Hung, K.-Y.; Lin, Y.-C.; Feng, H.-P. The Effects of Acid Etching on the Nanomorphological Surface Characteristics and Activation Energy of Titanium Medical Materials. *Materials* **2017**, *10*, 1164. [[CrossRef](#)]
44. Surmeneva, M.A.; Khrapov, D.; Prosolov, K.; Kozadayeva, M.; Koptuyug, A.; Volkova, A.; Paveleva, A.; Surmenev, R.A. The influence of chemical etching on porous structure and mechanical properties of the Ti6AL4V Functionally Graded Porous Scaffolds fabricated by EBM. *Mater. Chem. Phys.* **2022**, *275*, 125217, ISSN 0254-0584. [[CrossRef](#)]
45. Bright, R.; Hayles, A.; Wood, J.; Ninan, N.; Palms, D.; Visalakshan, R.M.; Burzava, A.; Brown, T.; Barker, D.; Vasilev, K. Bio-Inspired Nanostructured Ti-6Al-4V Alloy: The Role of Two Alkaline Etchants and the Hydrothermal Processing Duration on Antibacterial Activity. *Nanomaterials* **2022**, *12*, 1140. [[CrossRef](#)]
46. ASTM B214-16; Standard Test Method for Sieve Analysis of Metal Powders. ASTM: West Conshohocken, PA, USA, 2016; Volume 02.05.
47. ASTM F2924-14; Standard Specification for Additive Manufacturing Titanium-6 Aluminum-4 Vanadium with Powder Bed Fusion. ASTM: West Conshohocken, PA, USA, 2014; Volume 10.04.
48. ASTM F1472-08; Standard Specification for Wrought Titanium-6Aluminum-4Vanadium Alloy for Surgical Implant Applications. ASTM: West Conshohocken, PA, USA, 2008; Volume 10.15.
49. Yazid, F.; Kay, A.N.M.; Qin, W.Y.; Luchman, N.A.; Wahab, R.M.A.; Ariffin, S.H.Z. Morphology and Osteogenic Capability of MC3T3-E1 Cells on Granular Hydroxyapatite Scaffold. *J. Biol. Sci.* **2019**, *19*, 201–209. [[CrossRef](#)]
50. Jimenez, E.H.; Kreitberg, A.; Moquin, E.; Brailovski, V. Influence of Post-Processing Conditions on the Microstructure, Static, and Fatigue Resistance of Laser Powder Bed Fused Ti-6Al-4V Components. *J. Manuf. Mater. Process.* **2022**, *6*, 85. [[CrossRef](#)]
51. Chen, A.; Li, Y.; Zhao, X.; He, H.; Sun, G.; Li, W.; Wang, X. Spray-deposited Ag nanoparticles on micro/nano structured Ti6Al4V surface for enhanced bactericidal property and cytocompatibility. *Surf. Coat. Technol.* **2022**, *431*, 128010, ISSN 0257-8972. [[CrossRef](#)]
52. Obeidi, M.A.; Mussatto, A.; Dogu, M.N.; Sreenilayam, S.P.; McCarthy, E.; Ul Ahad, I.; Keaveney, S.; Brabazon, D. Laser surface polishing of Ti-6Al-4V parts manufactured by laser powder bed fusion. *Surf. Coat. Technol.* **2022**, *434*, 128179, ISSN 0257-8972. [[CrossRef](#)]
53. Damiati, L.; Eales, M.G.; Nobbs, A.H.; Su, B.; Tsimbouri, P.; Salmeron-Sanchez, M.; Dalby, M. Impact of surface topography and coating on osteogenesis and bacterial attachment on titanium implants. *J. Tissue Eng.* **2018**, *9*, 2041731418790694. [[CrossRef](#)] [[PubMed](#)]
54. Ginestra, P.; Ceretti, E.; Lobo, D.; Lowther, M.; Cruchley, S.; Kuehne, S.; Villapun, V.; Cox, S.; Grover, L.; Shepherd, D.; et al. Post Processing of 3D Printed Metal Scaffolds: A Preliminary Study of Antimicrobial Efficiency. *Procedia Manuf.* **2020**, *47*, 1106–1112. [[CrossRef](#)]

Disclaimer/Publisher's Note: The statements, opinions and data contained in all publications are solely those of the individual author(s) and contributor(s) and not of MDPI and/or the editor(s). MDPI and/or the editor(s) disclaim responsibility for any injury to people or property resulting from any ideas, methods, instructions or products referred to in the content.